EJN fens EUROPEAN JOURNAL OF NEUROSCIENCE

European Journal of Neuroscience, Vol. 36, pp. 1971–1983, 2012 doi:10.1111/j.1460-9568.2012.08080.x

SYNAPTIC MECHANISMS

Altered profile of basket cell afferent synapses in hyper-excitable dentate gyrus revealed by optogenetic and two-pathway stimulations

Marco Ledri[1], Litsa Nikitidou[1], Ferenc Erdelyi,[2] Gabor Szabo[2], Deniz Kirik[3], Karl Deisseroth[4] and Merab Kokaia[1]
[1]Experimental Epilepsy Group, Division of Neurology, Wallenberg Neuroscience Centre, Lund University Hospital, Lund, Sweden
[2]Department of Gene Technology and Developmental Neurobiology, Institute for Experimental Medicine, Budapest, Hungary
[3]Brain Repair and Imaging in Neural Systems (BRAINS) Unit, Department of Experimental Medical Sciences, Lund University Hospital, Lund, Sweden
[4]Department of Bioengineering, Department of Psychiatry and Behavioral Sciences, Stanford University, Stanford, CA, USA

Keywords: cholecystokinin, hippocampus, mouse, neuropeptide Y, synaptic transmission

Abstract

Cholecystokinin (CCK-) positive basket cells form a distinct class of inhibitory GABAergic interneurons, proposed to act as fine-tuning devices of hippocampal gamma-frequency (30–90 Hz) oscillations, which can convert into higher frequency seizure activity. Therefore, CCK-basket cells may play an important role in regulation of hyper-excitability and seizures in the hippocampus. In normal conditions, the endogenous excitability regulator neuropeptide Y (NPY) has been shown to modulate afferent inputs onto dentate gyrus CCK-basket cells, providing a possible novel mechanism for excitability control in the hippocampus. Using GAD65-GFP mice for CCK-basket cell identification, and whole-cell patch-clamp recordings, we explored whether the effect of NPY on afferent synapses to CCK-basket cells is modified in the hyper-excitable dentate gyrus. To induce a hyper-excitable state, recurrent seizures were evoked by electrical stimulation of the hippocampus using the well-characterized rapid kindling protocol. The frequency of spontaneous and miniature excitatory and inhibitory post-synaptic currents recorded in CCK-basket cells was decreased by NPY. The excitatory post-synaptic currents evoked in CCK-basket cells by optogenetic activation of principal neurons were also decreased in amplitude. Interestingly, we observed an increased proportion of spontaneous inhibitory post-synaptic currents with slower rise times, indicating that NPY may inhibit gamma aminobutyric acid release preferentially in peri-somatic synapses. These findings indicate that increased levels and release of NPY observed after seizures can modulate afferent inputs to CCK-basket cells, and therefore alter their impact on the oscillatory network activity and excitability in the hippocampus.

Introduction

Hippocampal basket cells form a distinct class of interneurons that provide inhibition to the cell bodies and proximal dendrites of principal cells. The spatial segregation and strategic location of their efferents enable efficient control of the output of principal neurons and consequently regulate oscillation rate, spike timing and activity synchronization of their targets (Cobb *et al.*, 1995; Ylinen *et al.*, 1995; Miles *et al.*, 1996). Two main populations of basket cells have been described in all major areas of the hippocampus (Somogyi & Klausberger, 2005). These two populations have similar morphological appearance but express diverse protein markers and differ in functional characteristics. They can be distinguished by expression of either the calcium binding protein parvalbumin (PV) or the neuropeptide cholecystokinin (CCK) (Freund & Katona, 2007). PV-positive basket cells are proposed to act as clockwork devices for the induction of learning-related gamma-frequency (30–90 Hz) oscillations due to their ability to generate high-frequency APs and to release gamma aminobutyric acid (GABA) in a synchronous manner (Freund, 2003). In contrast, APs of CCK-basket cells are characterized by strong accommodation, the cells express a variety of receptors for modulatory neurotransmitters (e.g. 5-hydroxytryptamine 3, nicotinic alpha4 and alpha7, and cannabinoid 1 receptors) (Freedman *et al.*, 1993; Katona *et al.*, 1999; Porter *et al.*, 1999; Ferezou *et al.*, 2002), and are thought to act as fine-tuning devices that modulate high-frequency network activity (Freund, 2003). As gamma-frequency oscillations can convert into higher frequency epileptiform activity (Traub *et al.*, 2005) in hyper-excitable states, CCK-basket cells could play an important role in this conversion. In line with this notion, the endogenous factors that regulate hippocampal excitability, e.g. neuropeptide Y (NPY), also can modulate synaptic drive onto the CCK-basket cells (Ledri *et al.*, 2011). During the hyper-excitable state in animals (animal models of epilepsy) and in patients with temporal lobe epilepsy, numerous alterations of synaptic efficacy, network connectivity and other structural reorganizations occur (cell death, axonal sprouting, syna-

Correspondence: Dr M. Kokaia, as above.
E-mail: merab.kokaia@med.lu.se

Received 9 February 2012, revised 14 February 2012, accepted 15 February 2012

ptogenesis, neurogenesis, inflammation, etc.). Various subtypes of interneurons undergo cell death and their network connectivity is altered (Bausch, 2005). Of particular interest is that expression of NPY and its receptors also undergo considerable changes. After induction of seizures, NPY and Y2 receptor expression have been found to be up-regulated in hilar interneurons, dentate granule cells and mossy fibers (Marksteiner *et al.*, 1990; Gruber *et al.*, 1994; Schwarzer *et al.*, 1998; Vezzani *et al.*, 1999), while Y1 receptor expression in the dentate granule cell dendrites is down-regulated (Kofler *et al.*, 1997). Therefore, we hypothesized that afferent synaptic inputs onto CCK-basket cells are likely to be modulated by endogenous excitability regulators such as NPY, and may play a role in normalizing hyper-excitability and high-frequency activity during seizures.

Materials and methods

Animals

A total of 95 young adult glutamic acid decarboxylase 65-enhanced green fluorescent protein (GAD65-GFP) mice were used (Brager *et al.*, 2003), of both sexes, at the age of 7–8 weeks at the time of the beginning of the experimental procedures. Mice were maintained in a FVB/N background. Breeding was conducted between heterozygote transgenic males and wild-type FVB/N females. In this transgenic line, GFP is expressed under the control of the GAD65 promoter, allowing visual identification of several populations of inhibitory interneurons, including CCK-basket cells. All experiments were conducted according to international guidelines on the use of experimental animals, as well as the Swedish Animal Welfare Agency guidelines, and were approved by the local Ethical Committee for Experimental Animals.

Production of recombinant adeno-associated viral (AAV) vectors

An AAV-CamKIIa-ChR2-mCherry expression vector was constructed by excising (*Xba*I, *Eco*RI) the CamKIIa-ChR2-mCherry portion of a lentiviral construct and cloning it in an AAV backbone vector containing the woodchuck post-transcriptional regulatory element (WPRE) and the human growth hormone polyadenilation (hGH-polyA) sequences flanked by inverted terminal repeats (ITRs). Virus production was essentially performed as previously described (Eslamboli *et al.*, 2005), with minor modifications. Briefly, the transfer vector and the packaging plasmid, pDG5, were transfected into 293 cells. Seventy hours after transfection the cells were harvested and lysed using one freeze–thaw cycle. The crude lysate was clarified by centrifugation at 4500 ***g*** for 20 min and the vector-containing supernatant was purified using a iodixanol gradient and ultracentrifugation (1.5 h at 350 000 ***g***). The virus-containing iodixanol gradient fraction was further purified using an Acrodisc Mustang Q device (Pall Life Sciences, Port Washington, NY, USA). For further concentration, desalting and buffer exchange, the purified vector suspension was centrifuged in an Amicron Ultra device (Millipore). The AAV vector was produced as serotype 5. The final number of AAV particles was determined using quantitative PCR and was 7.4×10^{12} genomic particles/mL.

Electrode implantation and virus injection

Animals were anesthetized by inhalation of isofluorane (2.5%; Baxter Chemical AB) and fixed onto a stereotaxic frame (David Kopf Instruments, Tujunga, CA, USA). A bipolar stainless steel stimulation/recording electrode (Plastics One, Roanoke, VA, USA) was stereotaxically implanted in the ventral right hippocampus at the following coordinates (in mm): AP −2.9, ML 3.0, DV −3.0. A reference electrode was placed in the temporal muscle. Electrodes were placed into a pedestal (Plastics One) and fixed on the skull with dental cement (Kemdent).

In a subset of animals, during the same surgery, AAV-CamKIIa-ChR2-mCherry viral vector suspension was injected through a glass capillary in the left hippocampus (contralateral to the electrode) at the following coordinates (in mm): AP −3.2, ML −3.1, DV −3.6 and −3.2. A 0.5-μL aliquot of viral suspension was injected at 0.1 μL/min in each location in the DV plane. The glass pipette was left in place for 5 min after each injection to avoid back-flow of viral particles through the injection tract. Reference points for stereotaxic surgery were bregma for the AP axis, midline for the ML axis and dura for the DV axis.

Electrical rapid kindling and test stimulations

At 7 days after electrode implantation and virus injection, the animals were subjected to electrical rapid kindling in the hippocampus, as previously described (Elmer *et al.*, 1996; Sorensen *et al.*, 2009). The individual threshold was determined by delivering stimulations (1-s train consisting of 1-ms bipolar square wave pulses at 100 Hz) of increasing current in 10-μA steps until a focal epileptiform afterdischarge (AD) of more than 5-s duration was detected by electroencephalographic (EEG) recording. During rapid kindling induction, EEG activity was continuously recorded on a MacLab system (ADInstruments, Bella Vista, Australia) for 200 min except during stimulations, which consisted of 40 suprathreshold stimulation trains (10 s, 1-ms square wave pulses at 50 Hz, 400-μA intensity) separated by 5 min between stimulations. Behavioral seizures were scored according to the Racine scale (Racine, 1972): grade 0, arrest, normal behavior; grade 1, facial twitches (nose, lips, eyes); grade 2, chewing, head nodding; grade 3, forelimb clonus; grade 4, rearing, falling on forelimbs; grade 5, imbalance and falling on side or back. Only animals that developed at least six stage 3–5 seizures were subsequently used for electrophysiology.

To assess if animals achieved a hyper-excitable state at the time point of electrophysiology, 4 weeks after the first kindling the individual threshold was re-measured in a subset of animals (n = 5). Animals were then given five additional stimulations using the same parameters of the first five kindling stimulations. Seizure grades and AD duration were assessed as previously described (Elmer *et al.*, 1996; Sorensen *et al.*, 2009).

Slice preparation

Four to six weeks after stimulations, animals were briefly anesthetized with isofluorane and decapitated. The head was quickly immersed in chilled sucrose-based cutting solution, containing (in mM): sucrose 75, NaCl 67, $NaHCO_3$ 26, glucose 25, KCl 2.5, NaH_2PO_4 1.25, $CaCl_2$ 0.5, $MgCl_2$ 7 (pH 7.4, osmolarity 305–310 mOsm). The brain was removed and placed in a Sylgard-coated Petri dish containing chilled sucrose-based solution, the cerebellum was discarded and the two hemispheres were divided using a razor blade. The left hemisphere, contralateral to the stimulating electrode, was then positioned lying on the medial side and a 'magic-cut' was performed on the dorsal cortex (Bischofberger *et al.*, 2006). The tissue was subsequently glued 'magic-cut' side down on a pedestal and transferred to a cutting chamber containing sucrose-based solution maintained at 2–4 °C and constantly oxygenated with carbogen (95% O_2/5% CO_2). Transverse slices 300 μm thick,

comprising the hippocampus and entorhinal cortex, were cut on a vibrating microtome (VT1200S; Leica Microsystems, advancing speed was set at 0.05 mm/s and amplitude at 1.7 mm), and immediately transferred to an incubation chamber containing sucrose-based solution constantly oxygenated with carbogen (95% O_2/5% CO_2) and maintained at 34 °C in a water bath. Slices were allowed to rest for 30 min before being transferred to room temperature and processed for electrophysiology.

Whole-cell patch-clamp electrophysiology

Individual slices were placed in a submerged recording chamber constantly perfused with gassed artificial cerebrospinal fluid (aCSF) containing, in mM: NaCl 119, $NaHCO_3$ 26, glucose 25, KCl 2.5, NaH_2PO_4 1.25, $CaCl_2$ 2.5 and $MgSO_4$ 1.3 (pH 7.4, osmolarity 305–310 mOsm). The temperature in the recording chamber was maintained at 32–34 °C, unless otherwise noted. GAD65-GFP-positive cells were visualized under fluorescent light and infrared differential interference contrast microscopy was used for visual approach of the recording pipette. Recording pipettes (2.5–5 MΩ resistance) were pulled from thick-walled (1.5 mm outer diameter, 0.86 mm inner diameter) borosilicate glass with a Flaming-Brown horizontal puller (P-97; Sutter Instruments, CA, USA), and contained (in mM): K-gluconate 122.5, KCl 12.5, KOH-HEPES 10, KOH-EGTA 0.2, MgATP 2, Na_3GTP 0.3, NaCl 8 (pH 7.2–7.4, 300–310 mOsm) for measurements of intrinsic properties and for monitoring the response to light in channelrhodopsin-2 (ChR2)-expressing cells; Cs-gluconate 117.5, CsCl 17.5, NaCl 8, CsOH-HEPES 10, CsOH-EGTA 0.2, MgATP 2, Na_3GTP 0.3, QX-314 5 (pH 7.2–7.4, 300–310 mOsm) for spontaneous, miniature and light-evoked excitatory post-synaptic currents recordings (sEPSCs, mEPSCs and leEPSCs, respectively); CsCl 135, CsOH 10, CsOH-EGTA 0.2, MgATP 2, Na_3GTP 0.3, NaCl 8, QX-314 5 (pH 7.2–7.4, 300–310 mOsm) for spontaneous, miniature and dual stimulation-evoked inhibitory post-synaptic currents recordings (sIPSCs, mIPSCs and dsIPSCs, respectively). Biocytin (3–5 mg/mL) was routinely added to the pipette solution on the day of the recording. Recordings typically lasted 20–30 min, and biocytin was allowed to diffuse for an additional 10 min at the end to ensure complete diffusion in the axonal arbor. Uncompensated series resistance (typically 8–30 MΩ) was constantly monitored via −5-mV voltage steps and recordings were discontinued after changes of > 20% or if the resting membrane potential was more positive than −50 mV.

Cells were held at −70 mV in voltage clamp and at 0 pA in current clamp recordings. Firing pattern and accommodation were investigated by applying a single 1-s, 500-pA depolarizing current step. Action potential threshold, amplitude and rheobase were measured by the first AP of the train evoked with a 1-s voltage ramp of 0–300 or 0–500 pA. The current–voltage relationship was analysed by injecting consecutive incremental 500-ms 10-pA current steps, from −200 to +200 pA.

EPSCs were recorded in the presence of 100 μM picrotoxin (PTX; Tocris Bioscience, Ellisville, MI, USA) to block gamma-aminobutyric acid A ($GABA_A$) receptors. Fifty micromolar DL-2-amino-5-phosphonovaleric acid (D-AP5; Tocris) and 5 μM 2,3-dihydroxy-6-nitro-7-sulfamoyl-benzo[f]quinoxaline-2,3-dione (NBQX; Tocris) were used during IPSC recordings to block *N*-methyl-D-aspartate (NMDA) and α-amino-3-hydroxy-5-methylisoxazole-4-propionic acid (AMPA) receptors, respectively. For mEPSC and mIPSC recordings, 1 μM tetrodotoxin (TTX; Tocris) was used to block voltage-gated sodium channels and prevent generation of APs. The specific metabotropic group II receptor (mGluR II) agonist (2S,1′S,2′S)-2-(Carboxycyclopropyl)glycine (L-CCG-I, 10 μM; Tocris) was used to activate mGluR II, which are exclusively expressed presynaptically on mossy fibers, to selectively block glutamate release from mossy fibers and respective mossy fiber-specific EPSCs in postsynaptic neurons (Kokaia *et al.*, 1998).

For light-evoked EPSC recordings, a 400-μm-thick optical fiber was positioned above the apex of the dentate gyrus. Light was generated by a 460-nm wavelength LED light source (WT&T Technology, Quebec, Canada) and stimulation of pre-synaptic ChR2-expressing cells was achieved via paired 1- to 2-ms light pulses with 50-ms inter-stimulation-interval (ISI) at 0.06 Hz.

For dual stimulation-evoked IPSCs, two bipolar stainless steel stimulating electrodes were placed in the outer molecular layer and in the granule cell layer of the dentate gyrus, respectively. Paired-pulse stimulations were used at 0.06 Hz with 100-ms ISI.

NPY (Schafer-N, Copenhagen, Denmark) was dissolved in distilled water, stored in concentrated aliquots, diluted to 1 μM concentration in the perfusion solution immediately before use and allowed to diffuse in the recording chamber for 7 min before continuation of the recordings. The concentration of NPY used here has been previously shown to be the most effective in inhibiting Schaffer collateral-CA1 excitatory post-synaptic potentials in the hippocampus (Colmers *et al.*, 1987). Silicon-coated tubing and bottles were used to prevent the peptide from adhering to the tubing and container walls. PTX or D-AP5 and NBQX were applied at the end of the experiments to verify that the synaptic currents were generated by respective receptor activation.

Data were sampled at 20 kHz with an EPC-10 amplifier (HEKA Elektronik, Lambrecht, Germany) and stored on a G4 Macintosh computer using PatchMaster software (HEKA) for offline analysis.

Immunohistochemistry and axonal arbor reconstruction

For identifying the cells recorded in this study, slices after electrophysiology were fixed in 4% paraformaldehyde (PFA) in phosphate buffer (PB) for 12–24 h and then stored in anti-freeze solution (ethylenglycol and glycerol in PB buffer) at −20 °C until processed. For immunohistochemical staining against GFP and biocytin, slices were rinsed three times with KPBS and pre-incubated for 1 h in blocking solution (10% normal goat serum and 0.25% Triton X-100 in KPBS, T-KPBS). Sections were then incubated overnight with 1 : 10 000 rabbit anti-GFP polyclonal antibody (ab1218; Abcam) in blocking solution, rinsed three additional times in T-KPBS and incubated for 2 h in FITC-conjugated goat anti-rabbit secondary antibody (1 : 400; Jackson Immunoresearch, Suffolk, UK) and Cy5-conjugated streptavidin (1 : 200; Jackson Immunoresearch) in blocking solution. Slices were finally rinsed three times in KPBS, mounted on coated slides and cover-slipped with DABCO. For evaluating the expression of AAV-CamKIIa-ChR2-mCherry, 1 : 1000 rat anti-mCherry (5F8; Chromotek, Germany) was added to the primary antibody incubation, and 1 : 400 Cy3-conjugated donkey anti-rat was added to the secondary antibodies.

For reconstruction of the axonal arborization, labeled neurons were examined with a confocal laser-scanning microscope (Leica). Confocal Z-stacks were obtained along the entire dendritic and axonal tree of the cells, and typically consisted of 40–50 planes.

Y2 immunohistochemistry and optical density measurements

To analyse the distribution of Y2 receptors, after fixation in 4% PFA overnight, slices from electrophysiological measurements and from

non-kindled GAD65-GFP age-matched controls were cryoprotected in 20% sucrose in PB for 2 days and additionally cut into 50-μm sections using a microtome. Sections were processed for Y2 immunohistochemistry essentially as previously described (Tu *et al.*, 2006). Briefly, slices were treated with 1% hydrogen peroxide for 30 min, pre-incubated for 1 h in blocking solution containing normal goat serum (see above), incubated for 24 h at 4 °C with 1 : 1000 rabbit anti-Y2 receptor antibody (RA14112; Neuromics, Edina, MN, USA) and subsequently with 1 : 500 biotinylated goat anti-rabbit secondary antibody (Vector Laboratories, UK). Y2 immunoreactivity was visualized by incubating the sections in avidin–biotin-conjugated horseradish peroxidase solution (ABC; Vector Laboratories), and then reacting them with 0.5 mg/mL diaminobenzidine (DAB), 0.025% cobalt chloride, 0.2% nickel ammonium sulfate and hydrogen peroxide solutions. Sections were finally dehydrated, mounted on coated slides and cover-slipped with Pertex (Histolab Products AB, Sweden).

Photomicrographs were taken from each section using the same exposure time and ambient light conditions, on the same day. To measure optical density of Y2-positive fibers, images were processed with ImageJ software (NIH, http://rsbweb.nih.gov/ij/). The density reading of the Y2-negative hippocampal fimbria structure was used as an internal reference for each section, and subtracted from the readings of the inner and outer molecular layers. Values for optical density are presented as arbitrary units.

Data analysis and statistics

Only cells resembling CCK-basket cells in morphology, with axonal arborization confined to the inner molecular and granule cell layers, and showing co-localization of GFP and biocytin were accepted for analysis. Off-line analysis was performed using FitMaster (HEKA Elektronik), IgorPro (Wavemetrics, Lake Oswego, OR, USA) and MiniAnalysis (Synaptosoft Inc., Decatur, GA, USA) software.

Action potential (AP) threshold was defined as the point where the fastest rising phase of the first AP in the ramp started. Rheobase was defined as the current needed in the ramp to reach AP threshold. AP amplitude and AP half-duration were defined as the difference between the threshold and the peak, in mV and ms, respectively. Paired-pulse facilitation and depression (PPF and PPD, respectively) were expressed as the ratio between the amplitude of the second and the first response of the pair, in percentage. Before and after NPY application, differences in resting membrane potential (RMP), AP threshold, AP amplitude, spontaneous and miniature current frequency and amplitude mean values, leEPSC and dsIPSC amplitudes, PPF and PPD were assessed with two-tailed Student's paired *t*-test using SPSS software (IBM). Optical density arbitrary unit measurements and stimulation-evoked IPSCs rise time comparisons were assessed with two-tailed Student's *t*-test. Inter-event-intervals (IEIs) and amplitude of spontaneous and miniature post-synaptic currents, and sIPSC rise times (10–90%) were analysed using MiniAnalysis software and differences between the groups were calculated with cumulative fraction curves combined with the Kolmogorov–Smirnov (*K-S*) test. Events were automatically recognized by the software and included in the analysis if their magnitude was at least five times bigger than the calculated average root mean square (RMS) noise. For sEPSC and mEPSC recordings, only the last 150 events before the start of NPY application and the first 150 events after equilibration of NPY (7 min after the start of NPY application) were included in the analysis. For sIPSC and mIPSC recordings, 200 events were included. Values are presented as means ± SEM. Differences are considered significant at $P < 0.05$ for Student's paired and un-paired *t*-test and $P < 0.01$ for the *K-S* test.

Results

Electrical rapid kindling and assessment of hyper-excitability

To induce hyper-excitability in the hippocampus, animals were subjected to rapid kindling stimulations (Elmer *et al.*, 1996; Sorensen *et al.*, 2009). During the 40 rapid kindling stimulations, animals developed seizures ranging from stage 0 to 5. The average number of stage 3–5 seizures was 12.7 ± 0.3 per animal. Four weeks later, at the time point for electrophysiological recordings, hyper-excitability was assessed in a subset of animals by delivering five additional rapid re-kindling stimulations. During re-kindling, the duration of afterdischarges at threshold stimulations was increased more than two-fold (68.0 ± 10.5 s for the re-kindling stimulations compared with 32.2 ± 5.0 s for the initial kindling, $n = 5$, $P = 0.036$, two-tailed Student's *t*-test), and the average number of stage 3–5 seizures was significantly higher (3.0 ± 0.2 for the re-kindling stimulations compared with 2.4 ± 0.4 for the initial five stimulations, $n = 5$, $P = 0.031$, two-tailed Student's *t*-test). These data show that, at the time point of electrophysiological recordings, the animals have developed a hyper-excitable state.

Identification of CCK-basket cells and effects of NPY on intrinsic membrane properties

In GAD65-GFP animals, several different subpopulations of GABAergic interneurons express GFP. To identify CCK-positive basket cells, the following morphological criteria were used, as previously described (Ledri *et al.*, 2011): (1) the cell soma had to be located on the border between the granule cell layer and the hilus, and (2) it had to be roughly pyramidal shaped; (3) the main apical dendrite had to reach the molecular layer and (4) the basal dendrites had to extend into the hilus (an example is shown in Fig. 1E–G). The cells displayed typical low-frequency, accommodating AP firing pattern upon depolarization (Fig. 1A and B), and their axonal arborization was mostly confined to the granule cell and inner molecular layers (Fig. 1D). These characteristics are consistent with the CCK-basket cell identity of the recorded cells.

We first investigated whether application of exogenous NPY could affect intrinsic membrane properties of CCK-basket cells in animals that have experienced recurrent seizures. The frequency of AP firing (Fig. 1A) and the degree of AP frequency accommodation (Fig. 1C) were not affected by NPY application, as well as the mean rheobase (Fig. 1B), resting membrane potential, AP threshold, amplitude and duration ($n = 6$, $P > 0.05$, two-tailed Student's paired *t*-test, Table 1). Thus, NPY does not seem to alter intrinsic membrane properties of CCK-basket cells in kindled animals.

The frequency of spontaneous and miniature EPSCs onto the CCK-basket cells is decreased by NPY

We next investigated whether NPY could modulate afferent excitatory synapses of the CCK-basket cells. We first recorded sEPSCs in voltage-clamp mode at −70 mV (with PTX in the perfusion solution to block $GABA_A$ receptors and pharmacologically isolate glutamate receptor-mediated currents) before and after application of 1 μM NPY. Figure 2A shows representative traces of sEPSCs recorded from CCK-basket cells. The mean frequency of sEPSCs was significantly

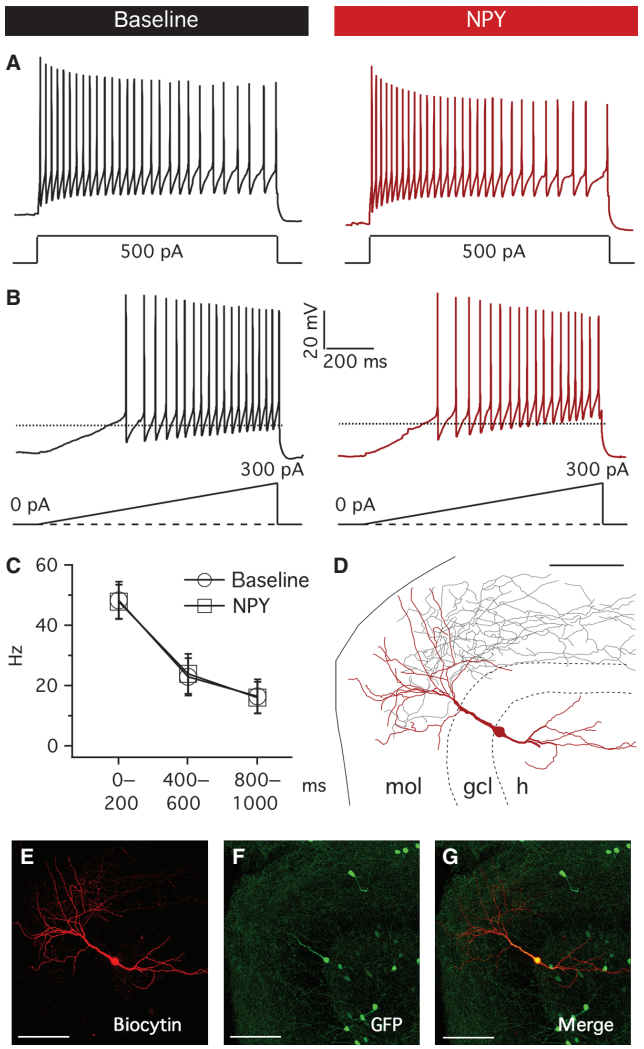

FIG. 1. NPY does not affect intrinsic membrane properties of CCK-basket cells in the dentate gyrus. (A) The typical regular-spiking accommodating response of a representative CCK-basket cell to a single 1-s, 500-pA depolarizing pulse injected through the patch pipette was not different between baseline (*left*, black trace) and after NPY application (*right*, red trace). (B) Representative traces showing the response of a CCK-basket cell to a current ramp consisting of 300 pA over 1 s. AP threshold (*dashed line*) and rheobase of CCK-basket cells did not differ before (*left*, black trace) and after (*right*, red trace) NPY application. (C) AP firing frequency and degree of frequency accommodation were not changed by NPY application. AP frequency was measured at three time points during the 1-s depolarization pulse as in A. (D) Neuronal reconstruction of a CCK-basket cell included in the study showing the typical distribution of dendritic (*red*) and axonal (*black*) arborizations. (E) The same cell as in D shows immunostaining for biocytin and GFP (F). Merged image is shown in G. Scale bars in D–G are 100 μm.

TABLE 1. NPY does not affect the intrinsic membrane properties of CCK-basket cells in the dentate gyrus of kindled animals

	Baseline (n = 6)	NPY (n = 6)
RMP (mV)	−57.5 ± 2.7	−56.2 ± 2.7
Input resistance (MΩ)	256.5 ± 51.8	244.5 ± 51.6
AP threshold (mV)	−35.0 ± 1.6	−36.2 ± 1.6
AP amplitude (mV)	72.9 ± 1.5	71.3 ± 2.2
AP half-duration (ms)	1.4 ± 0.1	1.6 ± 0.1
Rheobase (pA)	106.7 ± 25.5	93.3 ± 22.1

RMP, resting membrane potential; AP, action potential.

decreased by application of NPY (5.1 ± 0.6 Hz before and 3.9 ± 0.7 Hz after NPY application, n = 6, P = 0.008, two-tailed Student's paired t-test, Fig. 2B left) while the mean amplitude was not affected (17.9 ± 1.2 pA before and 19.4 ± 3.6 pA after NPY application, n = 6, P = 0.69, two-tailed Student's paired t-test, Fig. 2B right). The subsequent *K-S* analysis of the cumulative fraction of sEPSCs confirmed that the frequency was decreased (increase of IEIs, n = 6, $P < 0.001$, *K-S* test, Fig. 2C) and that the amplitude was not affected (n = 6, $P > 0.01$, *K-S* test, Fig. 2D). We then looked at whether the observed effect of NPY was due to decreased AP generation, and applied NPY while recording AP-independent mEPSCs by adding TTX in the perfusion solution to block voltage-gated sodium channels, and thereby APs, in all neurons. Figure 2E shows representative mEPSCs recordings. Similar to sEPSCs, the mean frequency of mEPSCs was decreased by application of NPY (4.2 ± 0.7 Hz before and 2.6 ± 0.4 Hz after NPY application, n = 5, P = 0.031, two-tailed Student's paired t-test, Fig. 2F left) but the mean amplitude was unaffected (17.6 ± 1.3 pA before and 18.0 ± 1.1 pA after NPY application, n = 5, P = 0.48, two-tailed Student's paired t-test, Fig. 2F right). The subsequent *K-S* analysis of the cumulative fraction for mEPSCs confirmed these results (Fig. 2G and H).

Taken together, these data demonstrate that NPY decreases the frequency of both AP-dependent and AP-independent EPSCs and suggest that NPY might act pre-synaptically by decreasing glutamate release.

Effects of NPY on short-term synaptic plasticity of EPSCs onto CCK-basket cells

The observed NPY-induced decrease in the frequency of both sEPSCs and mEPSCs could be explained by the reduction of pre-synaptic release probability (P*r*) of glutamate. An indirect indication of changes in P*r* could be obtained by measuring the ratio of EPSCs during paired-pulse stimulations. A paired-pulse facilitation (PPF) of EPSCs is a most common form of short-term synaptic plasticity observed in central excitatory synapses (Zucker & Regehr, 2002). An increase in PPF indicates decreased P*r*, while a decrease in PPF indicates an increase in P*r*. Therefore, possible effects of NPY on P*r* of glutamate in afferent excitatory synapses on CCK-basket cells were explored by evaluating afferent stimulation-induced PPF.

CCK-basket cells in the dentate gyrus receive numerous excitatory inputs: from granule cell mossy fiber collaterals on their basal dendrites in the hilus; from perforant path fibers on their apical dendrites in the molecular layer (Freund & Buzsaki, 1996); from hilar mossy cells (Scharfman, 1995), and possibly from CA3 pyramidal cells by axons back-propagating to the dentate gyrus (Scharfman, 2007). Current conventional electrical stimulation techniques do not allow for collective or selective studies on these excitatory inputs and their modulation. Therefore, we used optogenetics to explore excitatory inputs of the CCK-basket cells originating from all afferent synapses. To achieve this goal we used an optogenetic approach with ChR2. ChR2 is a microbial light-sensitive cation channel, which when expressed in the membrane of neurons and exposed to ~470 nm blue light is able to depolarize the cell membrane and generate APs in a very time-precise and controllable manner (Boyden *et al.*, 2005). Using AAV vectors, we expressed the ChR2 gene under the CamKIIa promoter in all populations of neurons producing afferent excitatory inputs onto the CCK-basket cells, as CamKIIa is selectively expressed in excitatory principal neurons in the hippocampus (CA1–CA3, dentate granule cells) and mossy cells in the dentate gyrus (Monory *et al.*, 2006). Thus, when activated by blue light, ChR2 generates

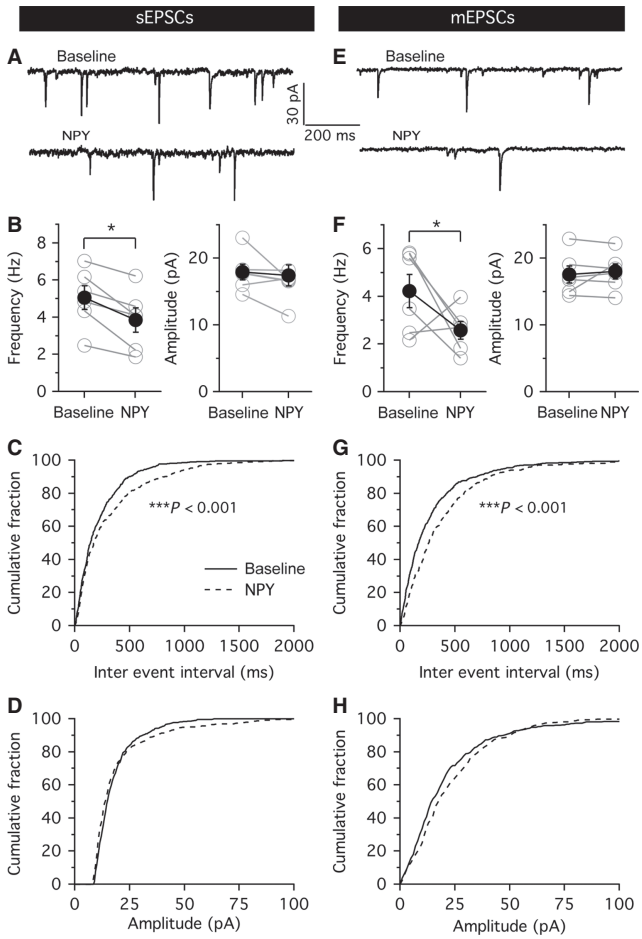

FIG. 2. NPY decreases the frequency of spontaneous and miniature EPSCs on CCK-basket cells but does not alter their amplitude. (A) Representative traces of sEPSCs recorded from CCK-basket cells during baseline (*top*) and after NPY application (*bottom*). (B) The mean frequency of sEPSCs was decreased by NPY application (*left*, $*P < 0.05$), but the amplitude was not changed (*right*, $P > 0.05$). Grey lines and open circles represent individual recordings, black lines and solid circles represent mean values. (C, D) Cumulative fraction analysis of inter event intervals (IEIs) and amplitudes of sEPSCs during baseline (*solid line*) and after NPY application (*dashed line*). IEIs were significantly increased by NPY application ($***P < 0.001$) while amplitudes were not affected ($P > 0.01$). (E) Representative traces of mEPSCs recorded from CCK-basket cells in the presence of 1 μM TTX before (*top*) and after (*bottom*) NPY application. Note the reduced frequency of events compared with sEPSCs (A). (F) NPY decreased the mean frequency of mEPSCs (*left*, $*P < 0.05$), but did not affect their amplitudes (*right*, $P > 0.05$). (G) Cumulative fraction curves showing that IEIs of mEPSCs were increased after NPY application ($***P < 0.001$), and (H) amplitudes were not affected ($P > 0.01$).

synchronous APs in all these populations of neurons at millisecond temporal precision. This results in EPSCs generated in CCK-basket cells from all excitatory inputs at the same time, a scenario that could very well be similar to what takes place during highly synchronized seizure activity in the hippocampus.

By using two injection sites targeting the ventral hippocampus, we could achieve robust and long-lasting expression of ChR2 in CA3 pyramidal cells, hilar mossy cells and dentate gyrus granule cells (Fig. 3A). In addition, fibers in the middle third of the molecular layer in the dentate gyrus and their cell bodies in layers II/III of the medial entorhinal cortex were also expressing ChR2 (Fig. 3A and E). The latter was consistent with the findings that AAV vectors can be transported retrogradely to the entorhinal cortex neurons by their axons in the molecular layer of the dentate gyrus (perforant path) (Kaspar *et al.*, 2002). This pattern of expression ensured that exclusively excitatory synapses onto the CCK-basket cells were activated by blue light illumination of the entire slice. Such selective stimulation of excitatory inputs would not be possible without an optogenetic approach.

To activate ChR2, we used a 400-μm core optical fiber connected to a 460-nm-wavelength LED light source, and placed it on the apex of the dentate gyrus, above the molecular layer (a schematic drawing of the experimental set-up is depicted in Fig. 3B). We then recorded from CCK-basket cells in voltage-clamp configuration at −70 mV. Two brief light stimulations, 1–2 ms in duration with an ISI of 50 ms, could reliably and efficiently generate APs in ChR2-positive cells (Fig. 4A, top) and evoke synaptic currents (leEPSCs) in the post-synaptic CCK-basket cells. All recorded paired leEPSCs exhibited PPF (Fig. 4A, bottom). Application of 1 μM NPY (Fig. 4B) caused more pronounced decrease in the amplitude of the first leEPSC (by 22.3% from baseline, $n = 13$, $P = 0.0001$, two-tailed Student's paired *t*-test) than of the second one (by 8.4% from baseline, $n = 13$, $P = 0.047$, two-tailed Student's paired *t*-test), resulting in an increase of the PPF (from 111.7 ± 6.7% before to 132.7 ± 9.3% after NPY application, $n = 13$, $P = 0.002$, two-tailed Student's paired *t*-test). NPY application did not affect the ability of ChR2 to induce APs in the pre-synaptic cells by light illumination ($n = 6$, $P > 0.05$, two-tailed Student's paired *t*-test, data not shown). These results indicate overall decreased P*r* of glutamate release from afferent synapses of CCK-basket cells.

To evaluate the relative contribution of granule cell mossy fiber-related excitatory inputs in the gross leEPSCs recorded in CCK-basket cells, we subsequently applied the selective mGluR II agonist L-CCG-I, which can suppress glutamate release selectively in mossy fibers of mice (Kokaia *et al.*, 1998; Armstrong *et al.*, 2002; Marchal & Mulle, 2004). The amplitude of both the first and the second leEPSCs of the pair was markedly decreased by L-CCG-I application (62.7 ± 3.7% of baseline for the first response, $P < 0.001$, and 68.0 ± 3.7% for the second, $P < 0.001$, $n = 11$, two-tailed Student's paired *t*-test, Fig. 4C) but the PPF ratio was unaltered (134.3 ± 8.4% before and 144.8 ± 7.7% after NPY application, $n = 11$, $P = 0.19$, two-tailed Student's paired *t*-test), indicating that mossy fiber contribution to the total leEPSCs was approximately 35%.

NPY decreases the frequency of sIPSCs and mIPSCs onto CCK-basket cells

Next we investigated whether NPY can modulate inhibitory synaptic transmission onto CCK-basket cells in hyper-excitable hippocampus. We started by recording sIPSCs in voltage-clamp configuration at −70 mV with NBQX and D-AP5 in the perfusion solution to block AMPA and NMDA glutamate receptors and isolate GABAergic transmission. Figure 5A shows representative traces of sIPSC recordings before and after NPY application. The mean frequency of sIPSCs was significantly decreased by application of NPY (from 5.9 ± 0.9 Hz before to 3.9 ± 0.8 Hz after NPY application, $n = 9$, $P = 0.046$, two-tailed Student's paired *t*-test, Fig. 5B left) but the mean amplitude was not affected (56.5 ± 6.4 pA before and 58.1 ± 5.7 pA after NPY application, $n = 9$, $P = 0.54$, two-tailed Student's paired *t*-test, Fig. 5B right). *K-S* analysis of the cumulative fraction confirmed that the sIPSC frequency was significantly decreased (as shown by the increase of IEIs, $n = 9$, $P < 0.001$, *K-S* test, Fig. 5C), while the amplitudes were not changed (Fig. 5D, $n = 9$, $P > 0.01$, *K-S* test).

To determine whether this effect of NPY was attributable to a decrease in AP firing of presynaptic GABAergic interneurons synapsing on CCK-basket cells, we blocked APs by adding TTX in the perfusion solution and recorded miniature IPSCs in CCK-basket

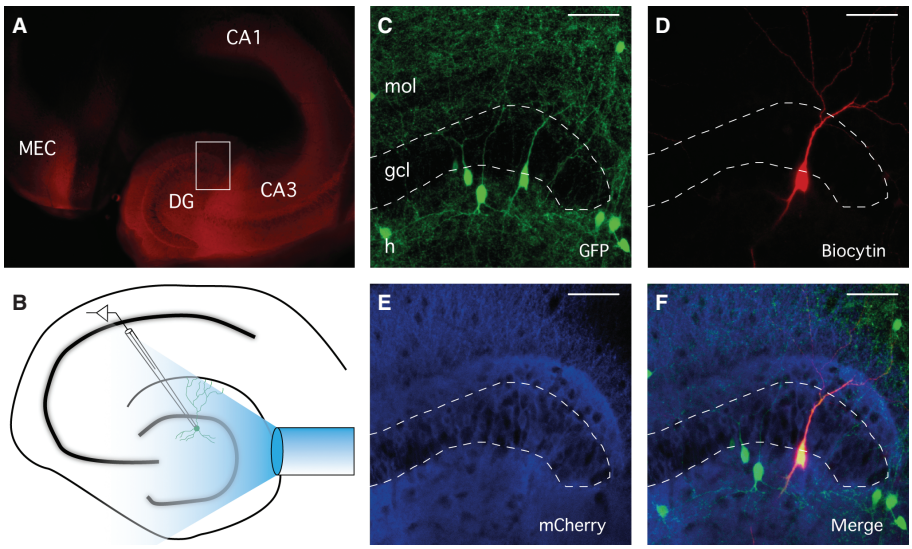

FIG. 3. Expression of AAV-CamKIIa-ChR2-mCherry in GAD65-GFP mice and experimental design. (A) Immunostaining against mCherry showing the extent of ChR2 expression in the hippocampus of virus-injected mice. Transgene expression was highest in the dentate gyrus (DG) and CA3 areas, but spread to CA1 and medial entorhinal cortex (MEC). (B) Schematic diagram depicting the experimental approach. A 400-μm-thick core optical fiber connected to a 460-nm blue LED light source was placed on top of the apex of the dentate gyrus to activate ChR2-expressing cells and fibers, while recordings were performed from GFP-positive CCK-basket cells. (C–F) Confocal stacks showing immunostaining against GFP (C), biocytin (D), mCherry (E) and merged images (F). Scale bars are 50 μm. *mol*, molecular layer; *gcl*, granule cell layer; *h*, hilus.

cells (Fig. 5E, note the lower amplitudes of mIPSCs compared with sIPSCs in Fig. 5A). In these conditions, NPY application still decreased the frequency of mIPSCs (from 4.3 ± 0.7 Hz before to 3.0 ± 0.5 Hz after NPY application, $n = 8$, $P = 0.017$, two-tailed Student's paired *t*-test, Fig. 5F left) without affecting the mIPSC amplitudes (42.3 ± 2.3 pA before and 45.5 ± 2.3 pA after NPY application, $n = 8$, $P = 0.23$, two-tailed Student's paired *t*-test, Fig. 5F right). *K-S* analysis of the cumulative fraction confirmed these results (Fig. 5G and H).

Taken together, these data suggest that NPY decreases pre-synaptic release of GABA, independently of APs, in afferent GABAergic synapses of CCK-basket cells.

NPY preferentially affects peri-somatic inhibitory synapses onto CCK-basket cells

CCK-basket cells receive inhibitory afferents from several different classes of GABAergic interneurons, including other CCK-basket cells, PV-positive basket cells and calretinin-positive interneuron-specific interneurons (CR-IS), at synapses across the entire dendritic tree (Nunzi *et al.*, 1985; Freund & Buzsaki, 1996; Gulyas *et al.*, 1996). The NPY-mediated decrease in the frequency of sIPSCs and mIPSCs described above does not indicate whether peri-somatic or distal dendritic inhibitory synapses are differentially modulated by NPY. Peri-somatic inhibitory synapses are thought to exert much stronger control over the ability of neurons to generate APs due to spatial shunting of excitatory currents originating mostly from the remote dendritic tree. Therefore, preferential modulation of peri-somatic inhibitory synapses by NPY would have greater consequences for the ability of the CCK-basket cells to generate APs. To address this, we analysed the relative contribution of sIPSCs and mIPSCs with fast and slow rise-time kinetics to the overall inhibitory drive onto the CCK-basket cells. Assuming that all IPSCs are generated by $GABA_A$ receptors which have similar activation–deactivation kinetics, and that GABA release kinetics in the synapses are also similar, a faster rise time of IPSCs would indicate that the current is generated by peri-somatic inhibitory synapses close to the recording electrode (placed on the cell soma), while a slower rise time of IPSCs would indicate dendritic localization further from the electrode (e.g. distal apical dendrites) (Kobayashi & Buckmaster, 2003). Frequency distribution histograms for sIPSCs indicated that the percentage of events with fast rise times (10–90%) were markedly decreased by NPY application (Fig. 6A), while for mIPSCs the curves for baseline and NPY application appeared largely overlapping (Fig. 6B). Quantitative *K-S* analysis of the cumulative fraction showed that both sIPSC and mIPSC rise times were significantly increased after NPY application compared with baseline (Fig. 6C and D, $n = 9$ for sIPSCs and $n = 8$ for mIPSCs, $P < 0.001$, *K-S* test), indicating that NPY might preferentially act on peri-somatic afferent inhibitory synapses of the CCK-basket cells. The detailed analysis also revealed that rise times of mIPSCs were slower than sIPSCs (notice the smaller peak during baseline in Fig. 6C compared with the same peak in Fig. 6A, black traces). Comparison of rise time values of sIPSCs and mIPSCs confirmed that mIPSCs were significantly slower, both during baseline conditions (Fig. 6E, $n = 9$ for sIPSCs and $n = 8$ for mIPSCs, $P < 0.001$, *K-S* test) and after NPY application (Fig. 6F, $n = 9$ for sIPSCs and $n = 8$ for mIPSCs, $P < 0.001$, *K-S* test), suggesting that those inhibitory interneurons that form peri-somatic synapses on CCK-basket cells are relatively more spontaneously active. Taken together, these data suggest that in the hyper-excitable hippocampus NPY acts primarily on those inhibitory synapses that are close to the cell soma of CCK-basket cells compared with those on the dendrites.

NPY decreases the amplitude of stimulation-evoked IPSCs

As the data described above suggest that NPY predominantly affects peri-somatic inhibitory synapses onto CCK-basket cells, we explored whether NPY was able to act also on distal/dendritic inhibitory synapses. To address this question, we placed stimulating electrodes in the granule cell layer (GCL, p1) of the dentate gyrus to stimulate peri-

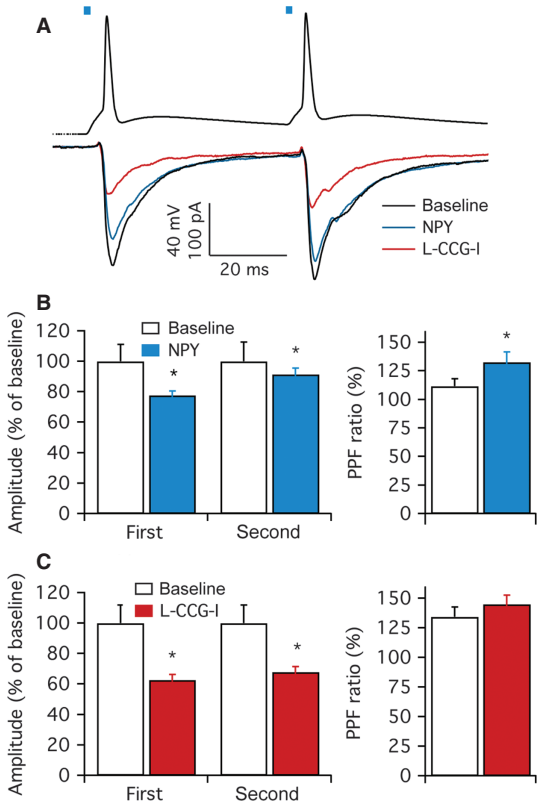

FIG. 4. Effects of NPY on light-evoked EPSCs recorded from CCK-basket cells. (A) *top*, representative trace (average of 16) showing the APs evoked by two paired 1-ms blue light pulses with 50-ms ISI in a ChR2-positive granule cell (blue lines on top indicate the moment of light stimulation); *bottom*, representative post-synaptic responses (average of 16) to blue light stimulations recorded in a CCK-basket cell in the presence of 100 μM PTX, during baseline (*black trace*), after NPY application (*blue trace*) and after application of 10 μM L-CCG-I (*red trace*). APs and post-synaptic responses were not recorded simultaneously. (B) *left*, mean amplitude of light-evoked EPSCs (leEPSCs). Both the first and the second response of the pair were significantly reduced by application of NPY (*blue bars*) compared with baseline (*white bars*) (*$P < 0.05$); *right*, the PPF ratio was significantly increased after NPY application (*$P < 0.05$). (C) Subsequent L-CCG-I application (*red bars*) further decreased the amplitude of leEPSCs (*left*, *$P < 0.05$), but left the PPF ratio unchanged (*right*, $P > 0.05$).

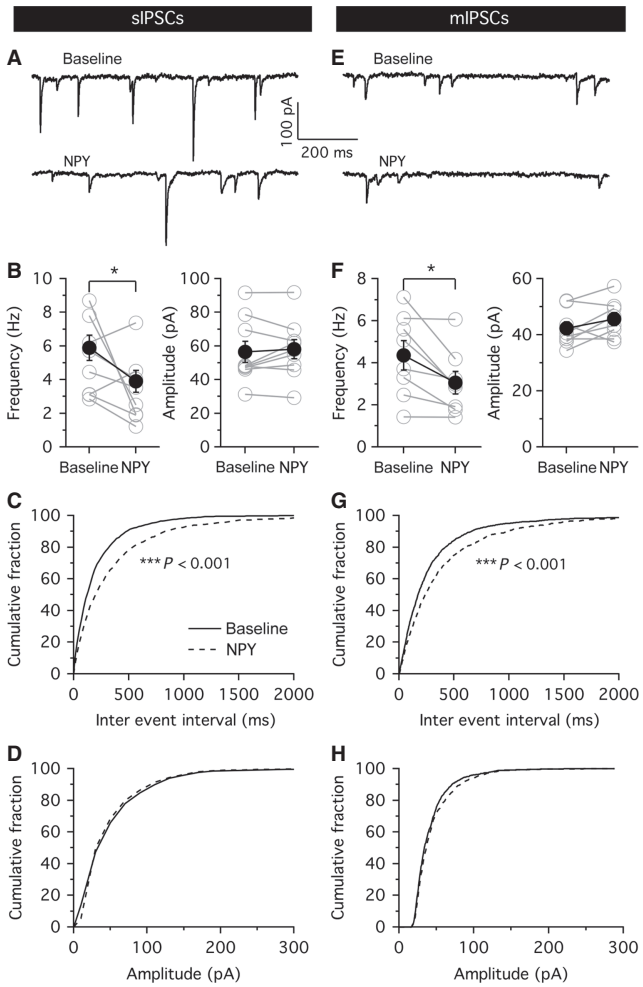

FIG. 5. NPY reduces the frequency of sIPSCs and mIPSCs recorded from CCK-basket cells. (A) Representative traces showing sIPSCs recorded during baseline (*top*) and after NPY application (*bottom*). (B) The mean frequency of sIPSCs was significantly decreased by NPY application (*left*, *$P < 0.05$), but the amplitude was not affected (*right*, $P > 0.05$). Grey lines and open circles represent individual recordings, black lines and solid circles represent mean values. (C) Cumulative fraction analysis showing an increase in the IEIs of sIPSCs after NPY application (*dashed line*) compared with baseline (*solid line*, ***$P < 0.001$). (D) Amplitudes of sIPSCs were not affected ($P > 0.01$). (E) Representative traces of mIPSCs recorded in the presence of 1 μM TTX during baseline (*top*) and after NPY application (*bottom*). Note the lower frequency and lower amplitudes of mIPSCs compared with sIPSCs in A. (F) NPY application significantly decreased the mean frequency of mIPSCs (*left*, *$P < 0.05$), but did not affect the mean amplitude (*right*, $P > 0.05$). (G) Cumulative fraction analysis confirming the observed decrease in mIPSC frequency after NPY application (increase of IEIs, ***$P < 0.001$), while amplitudes were not affected (H, $P > 0.01$).

somatic inhibitory afferent fibers to CCK-basket cells, and in the outer molecular layer (OML, p2) to stimulate distal dendritic afferent fibers (a schematic illustration of the experimental set-up is depicted in Fig. 7A). In the presence of NBQX and D-AP5 to block glutamate receptors and isolate monosynaptic GABAergic transmission, paired stimulations with 100-ms ISIs were delivered in both pathways, eliciting paired IPSCs, which expressed PPD (representative traces are shown in Fig. 7B and C). Application of NPY caused a significant and proportional decrease in the amplitude of IPSC pairs (for GCL stimulation, 85.2 ± 1.7% of baseline for the first response, $P = 0.018$, and 85.5 ± 2.7% of baseline for the second response, $P = 0.031$, Fig. 7C left, $n = 11$; for OML stimulation, 78.2 ± 3.8% of baseline for the first response, $P = 0.001$, and 78.6 ± 5.0% of baseline for the second response, $P = 0.011$, Fig. 7E left, $n = 10$; two-tailed Student's paired *t*-test). The PPD ratio was not altered (for GCL stimulation, 74.9 ± 2.7% during baseline and 74.8 ± 3.5% after NPY application, $n = 11$, $P = 0.98$, two-tailed Student's paired *t*-test, Fig. 7C right; for OML stimulation, 67.9 ± 4.9% during baseline and 67.9 ± 5.3% after NPY application, $n = 10$, $P = 0.99$, two-tailed Student's paired *t*-test, Fig. 7E right). Analysis of the rise times (10–90%) of the stimulation-evoked IPSCs revealed that the mean rise time of GCL-evoked IPSCs was significantly faster than that of OML-evoked IPSCs (for GCL stimulation, 4.7 ± 0.7 ms for the first response of the pair and 4.7 ± 0.6 ms for the second response, $n = 11$; for OML stimulation, 7.0 ± 0.9 ms for the first response and 6.8 ± 1.2 ms for the second response, $n = 10$; $P < 0.05$ in both cases, two-tailed Student's *t*-test, data not shown), confirming the spatial segregation of two different sets of afferent inhibitory synapses on CCK-basket cells (peri-somatic and dendritic, respectively) activated by this particular stimulation paradigm.

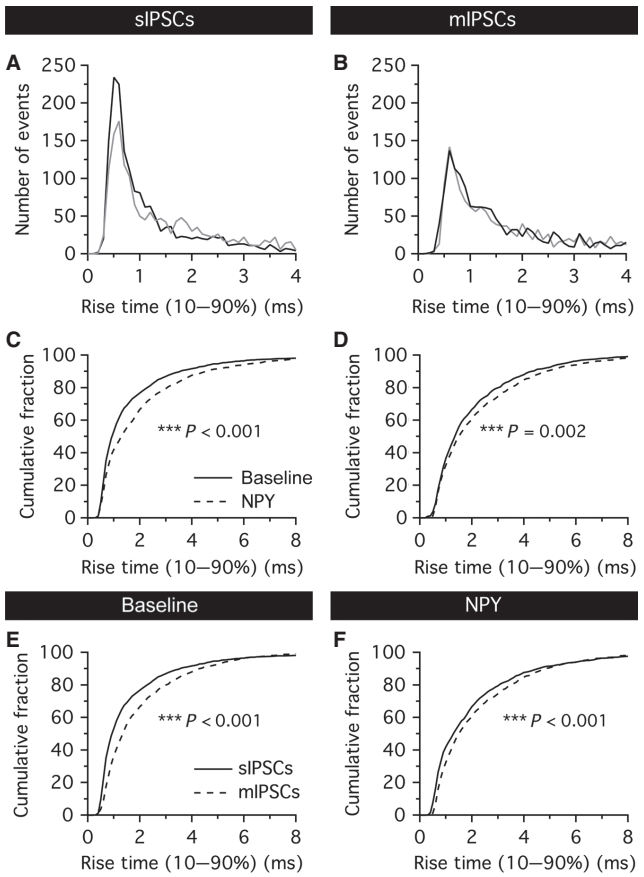

FIG. 6. NPY preferentially acts on peri-somatic inhibitory synapses onto CCK-basket cells. (A, B) Frequency distribution histograms of sIPSCs (A) and mIPSCs (B), before and after NPY application. NPY (*gray traces*) decreased the number of sIPSCs with fast rise time values compared with baseline (*black traces*), but curves for mIPSCs are largely overlapping. Note also the smaller peak during baseline in B compared with A. (C, D) Cumulative fraction analysis reveals that rise time values of both sIPSCs (C, $***P < 0.001$) and mIPSCs (D, $***P < 0.001$) are significantly increased by NPY application. (E, F) mIPSCs (*grey traces*) are significantly slower than sIPSCs (*black traces*), as indicated by larger rise time values, both during baseline (E, $***P < 0.001$) and after NPY application (F, $***P < 0.001$).

Y2 receptor expression is up-regulated after recurrent seizures

One possible explanation for the preferential action of NPY on peri-somatic inhibitory afferent synapses of CCK-basket cells could be a re-distribution of presynaptic NPY receptors in these terminals caused by hyper-excitable conditions of the hippocampus. Between the three NPY receptors highly expressed in the hippocampus (Y1, Y2 and Y5), we chose to study the distribution of Y2 receptors, which we have previously shown to be involved in the regulation of inhibitory synapses onto CCK-basket cells by NPY (Ledri *et al.*, 2011).

We performed immunohistochemistry for Y2 receptor distribution in slices from hyper-excitable animals and age-matched controls, and analysed the immunoreactive fiber density in the inner and outer molecular layers of the dentate gyrus. Representative immunostainings of slices from both groups are shown in Fig. 8A and B. Immunoreactive fiber density (optical densitometry) analysis revealed that Y2 expression in hyper-excitable animals was significantly increased in the inner molecular layer of the dentate gyrus (34.6 ± 3.2 AU in the normal, $n = 14$, and 60.2 ± 8.6 AU in the kindling animals, $n = 11$, corresponding to an increase of 74.0 ± 12.0%, Fig. 8C IML; $P < 0.001$, two-tailed Student's *t*-test). Overall Y2 expression was

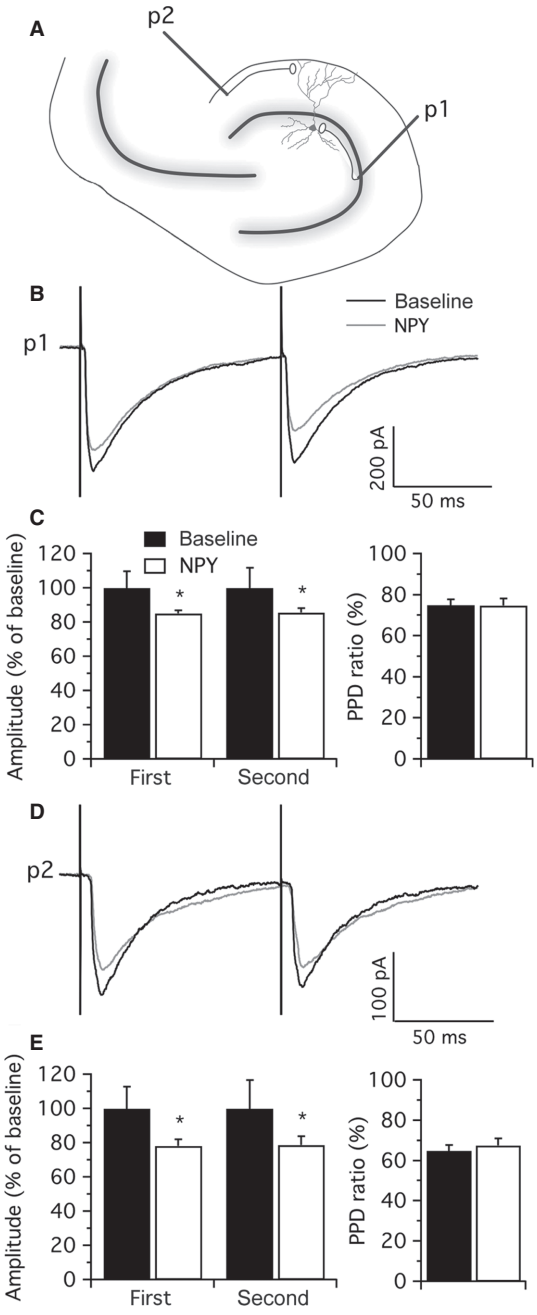

FIG. 7. NPY decreases the amplitude of peri-somatic and dendritic stimulation-induced IPSCs. (A) Schematic illustration of the experimental set-up. Bipolar stimulating electrodes were placed in the granule cell layer (GCL, p1), to activate peri-somatic inhibitory synapses, and in the outer molecular layer (OML, p2), to activate dendritic inhibitory synapses, while recording from CCK-basket cells in the presence of 5 μM NBQX and 50 μM D-AP5. Paired pulses were delivered in both pathways with 100-ms ISI. (B) Representative traces (average of 16) showing paired post-synaptic responses evoked by p1 stimulation, during baseline (*black trace*) and after NPY application (*grey trace*). (C) *left*, the amplitudes of both responses of the pair were significantly decreased by NPY application (*white bars*, $*P < 0.05$) compared with baseline (*black bars*); *right*, PPD ratio was unchanged ($P > 0.05$). (D) Representative traces (average of 16) showing paired responses evoked by p2 stimulation, during baseline (*black trace*) and after application of NPY (*grey trace*). (E) Application of NPY significantly decreased the amplitude of both the first and the second responses of the pair (*left*, $*P < 0.05$), but the PPD ratio was not altered (*right*, $P > 0.05$).

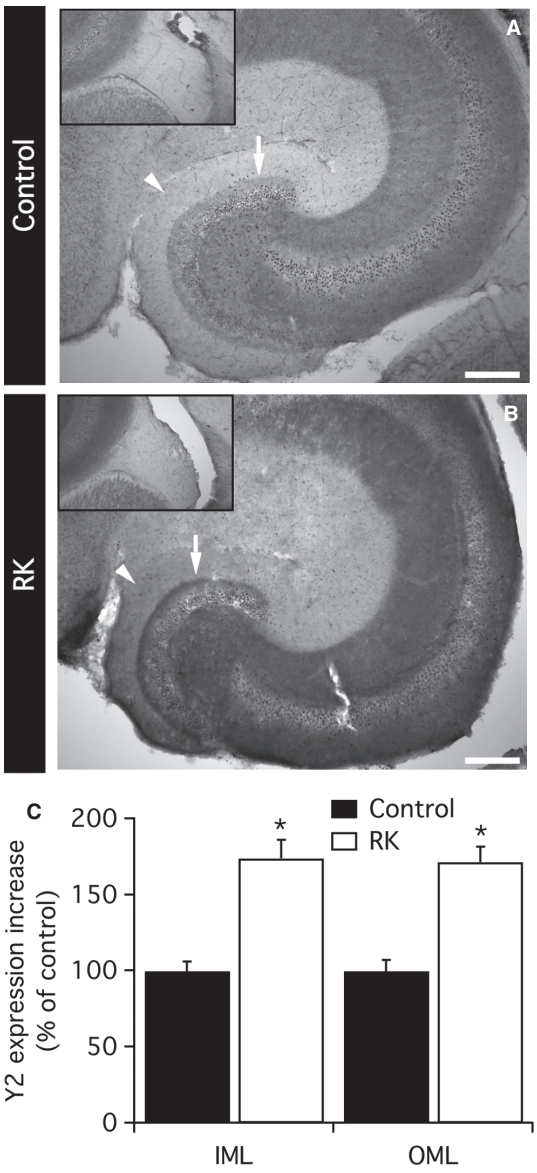

FIG. 8. Y2-immunopositive fiber density is increased in the hyper-excitable hippocampus. (A, B) Photomicrographs showing the distribution of Y2-positive fibers in the hippocampus of a control (A) and an animal that has been subjected to rapid kindling (RK, B). Arrow points to the inner molecular layer (IML), arrowhead to the outer molecular layer (OML). Insets to the top-left show the fimbria, used as reference in the optical density measurements. Scale bar = 100 μm. (C) Y2-positive fiber density in RK animals is significantly increased in both IML and OML of the dentate gyrus, compared with age-matched controls (*$P < 0.05$).

lower in the outer molecular layer of the control animals, and the increase tended to be slightly less pronounced in hyper-excitable animals (19.6 ± 1.5 AU in normal, $n = 14$, and 33.7 ± 2.4 AU in kindled animals, $n = 11$, corresponding to 71.5 ± 10.2% increase, Fig. 8C OML; $P < 0.001$, two-tailed Student's *t*-test). Comparisons between the reference optical density values measured in the fimbria showed no difference between the two groups (Fig. 8A and B, insets, $P > 0.05$, two-tailed Student's *t*-test, data not shown).

Discussion

Here, using optogenetic and two-pathway stimulation approaches, we demonstrate that in hyper-excitable hippocampus, afferent synapses on CCK-basket cells are altered and respond to the excitability modulator neuropeptide Y, by decreased probability of glutamate release and decreased inhibitory drive on peri-somatic area. This effect of NPY may impact AP generation probability in CCK-basket cells, and thereby downstream inhibition of principal cells.

Generation of hyper-excitability and identification of CCK-basket cells

In this study we explored whether hyper-excitable state of hippocampus alters afferent synapses to CCK-basket cells, which play a major role in modulating frequency oscillations and dentate gyrus excitability. To reveal such possible modifications, we challenged CCK-basket cell afferent synapses by the endogenous excitability modulator NPY, which is upregulated in and released from granule cells by seizure activity (Marksteiner *et al.*, 1990; Schwarzer *et al.*, 1998). We induced a hyper-excitable state in the hippocampus by exposing animals to a well-established rapid kindling stimulation protocol. The resulting hyper-excitability was assessed by stimulation-induced seizure susceptibility. Four weeks after the initial rapid kindling stimulations, at the time point of electrophysiological investigations, the animals displayed an increase in duration of afterdischarges elicited by threshold stimulations and an increased number of stage 3–5 seizures, consistent with previous results (Elmer *et al.*, 1996) demonstrating hyper-excitability.

To identify CCK-basket cells for electrophysiological recordings in GAD65-GFP mice, we used morphological criteria as previously described (Ledri *et al.*, 2011). Electrophysiological and morphological evidence convincingly demonstrated the CCK-basket cell identity of the recorded cells. Cells displayed regular-spiking phenotype and strongly accommodating AP trains, and the distribution of their axonal process was mostly confined to the granule cell and inner molecular layers, as previously described (Hefft & Jonas, 2005).

Moreover, we have shown that cells selected with these criteria express functional alpha7 nicotinic acetylcholine receptors and are immunoreactive for CCK (Ledri *et al.*, 2011).

Excitatory input onto CCK-basket cells

Application of NPY decreased the frequency of sEPSCs and mEPSCs recorded from CCK-basket cells. Changes in the frequency of spontaneous currents, but not in their amplitude, is usually indicative of processes affecting the pre-synaptic site, and therefore suggest an NPY-induced decrease of glutamate release in excitatory synapses onto CCK-basket cells. Supporting decreased glutamate release, the PPF ratio of EPSCs induced by optogenetic stimulation of afferents onto CCK-basket cells was increased by application of NPY, indicating a decreased glutamate P*r*.

CCK-basket cells receive excitatory inputs from mossy fiber collaterals on their basal dendrites in the hilus, perforant path and associational-commissural fibers (from mossy cells) on their apical dendrites in the molecular layer (Scharfman, 1995; Freund & Buzsaki, 1996). Some inputs also possibly arise from CA3 pyramidal cell axons back-projecting to the dentate gyrus (Scharfman, 2007). Our data show that at least some of these inputs are affected by NPY. Mossy fibers express Y2 receptors, as previously demonstrated by electrophysiology and immunohistochemistry (McQuiston & Colmers, 1996; Stanic *et al.*, 2006), and contribute to approximately 35% of the total excitatory input to CCK-basket cells (Fig. 4C). On the other hand, perforant path and associational fibers are thought to lack Y2 receptors, as NPY failed to alter stimulation-induced EPSPs and EPSCs recorded in the granule cell

layer and in single granule cells, respectively (Klapstein & Colmers, 1993). However, it is not known whether associational fiber synapses on interneurons differ from those on principal cells. The inner molecular layer, where associational fibers are arriving, do express Y2 receptors (Tu *et al.*, 2006) (Fig. 8), and therefore it cannot be excluded that NPY may act on these synapses as well.

Inhibitory input to CCK-basket cells

In the present study, NPY reduced the frequency of sIPSCs and mIPSCs recorded from CCK-basket cells in the hyper-excitable hippocampus. Such changes are attributable to a pre-synaptic site of action (Behr *et al.*, 2002). CCK-basket cells receive inhibitory input on their apical dendrites in the molecular layer, from HICAP and HIPP cells, and peri-somatically from PV- and CCK-basket cells (Nunzi *et al.*, 1985; Freund & Buzsaki, 1996). In addition, they receive inhibitory input in the inner molecular layer from a subtype of interneuron-specific interneurons positive for calretinin (CR-IS) (Gulyas *et al.*, 1996). Y2 receptor immunohistochemistry together with electrophysiological evidence suggests that synapses from CCK-basket cells and from CR-IS cells, both of which terminate in the inner molecular layer, may be affected by NPY, as this region seems to contain more Y2-immunoreactive fibers compared with the outer part of the molecular layer (Fig. 8A and B). In support of this, NPY shifted the rise time values of sIPSCs recorded from CCK-basket cells to lower values. The observed decrease in the frequency of sIPSCs does not seem to be exclusively related to inhibition of HIPP cells by NPY (Paredes *et al.*, 2003), as in our study the effect persisted in the presence of TTX.

Functional implications

CCK-basket cells are proposed to act as fine-tuning devices of network activity, partly due to the variety of modulatory receptors they selectively express. In particular, CCK-basket cells seem to be important in the regulation of learning-related gamma-frequency oscillations, which are thought to be generated by PV-basket cells and have been shown to convert into higher frequency epileptiform activity (Traub *et al.*, 2005). Taken together, our data support the idea that CCK-basket cells may play an important role in this frequency conversion. In support of this, we demonstrate that afferents to CCK-basket cells in hyper-excitable hippocampus are modulated by NPY, which is upregulated and/or is *de novo* expressed in some neuron populations (see below) by seizure activity, and is one of the most effective modulators of hippocampal excitability.

The hyper-excitable states of the brain, including epilepsy, are associated with massive changes in neuronal networks. Some interneuron subtypes undergo cell death, while synaptic connections to surviving interneurons are rearranged (Bausch, 2005). The expression of NPY and its receptors is also dramatically altered. NPY and Y2 receptors are up-regulated in granule cells, mossy fibers and hilar interneurons (Marksteiner *et al.*, 1990; Schwarzer *et al.*, 1998; Vezzani *et al.*, 1999), while Y1 expression is down-regulated in granule cell dendrites (Kofler *et al.*, 1997). As NPY acts as a volume transmitter, alterations in its expression and release patterns may change local access of CCK-basket cells to NPY, and thereby change the way they react to NPY released during high-frequency activity. This in turn would influence the overall impact of CCK-basket cells on the network, and possibly their modulatory action on network oscillations.

The observed effects of NPY on CCK-basket cell afferent synapses in the hyper-excitable environment can result in three possible scenarios.

(i) Because peri-somatic inhibitory synapses are strategically located to efficiently control the output of the post-synaptic neuron, the NPY-mediated decrease of peri-somatic inhibitory input onto CCK-basket cells might increase the probability of AP generation by CCK-basket cells, counteracting the parallel decrease in dendritic excitatory inputs. If decreased inhibitory peri-somatic drive prevails, it will result in increased output (and GABA release) from CCK-basket cells to pyramidal neurons (Fig. 9-1). Such action of NPY would favor normalization of increased excitability of the network.

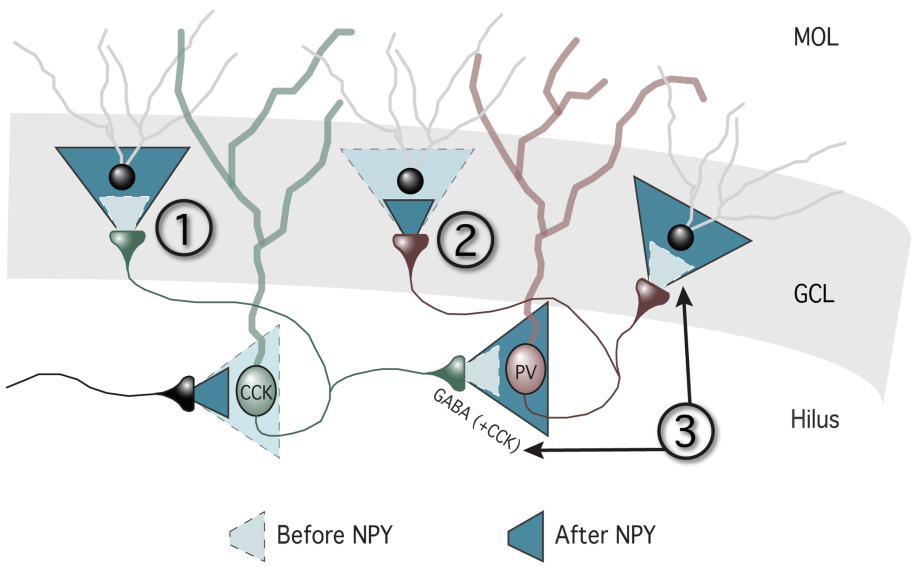

FIG. 9. Possible functional implications of the effect of NPY on CCK-basket cell afferents. Light blue and dashed lines represent baseline conditions, before NPY application. Dark blue and solid lines represent NPY-induced effects. Peri-somatic inhibitory inputs to CCK-basket cells are decreased by NPY application. This effect could result in three different scenarios: 1, GABA release from CCK-basket cells to dentate gyrus granule cells is increased; 2, increased inhibition of PV-basket cells by CCK-basket cells results in lowered granule cell inhibition by PV-basket cells; 3, increased CCK release from CCK-basket cells causes depolarization of PV-basket cells and increased synchronization of granule cells.

(ii) Inhibitory action on the network excitability exerted by release of GABA may not be the only mechanism by which inhibitory interneurons could regulate epileptiform activity and seizures (Avoli & de Curtis, 2011). Excessive synchrony of certain populations of interneurons, e.g. PV-basket cells, promoted by their highly synchronized GABA release, could support generation of epileptiform discharges. The CCK-basket cell axons are known to target not only granule cells but also PV-basket cells (Karson *et al.*, 2009). Therefore, increased inhibitory influence of CCK-basket cells on PV-basket cells due to the action of NPY would diminish the contribution of PV-basket cells in synchronizing pyramidal cell ensembles (Fig. 9-2). This could be an additional NPY-related mechanism by which CCK-basket cells would counteract development of high-frequency epileptiform activity.

(iii) Another alternative scenario could be envisaged in relation to release of CCK from CCK-basket cells during high-frequency activity in the hippocampus (Ghijsen *et al.*, 2001). In CA1, CCK has been shown to depolarize PV-basket cells, and increase their synchronizing impact onto CA1 pyramidal cells (Foldy *et al.*, 2007). Similarly, CCK has been shown to increase firing of hilar interneurons (Deng & Lei, 2006). In this scenario, higher probability of CCK-basket cell activation induced by NPY may lead to increased release of CCK, which consequently would depolarize PV-basket cells. This in turn could promote granule cell synchronization and development of epileptiform activity (Fig. 9-3).

Finally, further studies are needed to explore whether altered synaptic responsiveness of CCK-basket cells to NPY in hyper-excitable states is a *cause* or an *adaptive* response of the network to the hyper-excitability.

Acknowledgements

This work was supported by EU Commission grant NEUROTRAIN, EU Commission grant EPICURE, Segerfalk Foundation, Crafoord Foundation, Kock Foundation and Swedish Research Council. We thank Björn Anzelius for technical assistance with virus production. The authors declare no conflict of interest.

Abbreviations

aCSF, artificial cerebrospinal fluid; AMPA, α-amino-3-hydroxy-5-methylisoxazole-4-propionic acid; AP, action potential; CCK, cholecystokinin; ChR2, channelrhodopsin-2; DAB, diaminobenzidine; D-AP5, DL-2-amino-5-phosphonovaleric acid; EEG, electroencephalogram; GABA, gamma aminobutyric acid; GCL, granule cell layer; GFP, green fluorescent protein; IEI, inter event interval; IML, inner molecular layer; ISI, inter stimulus interval; L-CCG-I, (2S,1'S,2'S)-2-(carboxycyclopropyl)glycine; leEPSCs, light-evoked excitatory post-synaptic currents; mEPSCs, miniature excitatory post-synaptic currents; mIPSCs, miniature inhibitory post-synaptic currents; NBQX, 2,3-dihydroxy-6-nitro-7-sulfamoyl-benzo[f]quinoxaline-2,3-dione; NMDA, *N*-methyl-D-aspartate; NPY, neuropeptide Y; OML, outer molecular layer; PB, phosphate buffer; PFA, paraformaldehyde; PPD, paired pulse depression; PPF, paired pulse facilitation; PTX, picrotoxin; PV, parvalbumin; RMP, resting membrane potential; sEPSCs, spontaneous excitatory post-synaptic currents; sIPSCs, spontaneous inhibitory post-synaptic currents; TTX, tetrodotoxin.

References

Armstrong, J.N., Brust, T.B., Lewis, R.G. & MacVicar, B.A. (2002) Activation of presynaptic P2X7-like receptors depresses mossy fiber-CA3 synaptic transmission through p38 mitogen-activated protein kinase. *J. Neurosci.*, **22**, 5938–5945.

Avoli, M. & de Curtis, M. (2011) GABAergic synchronization in the limbic system and its role in the generation of epileptiform activity. *Prog. Neurobiol.*, **95**, 104–132.

Bausch, S.B. (2005) Axonal sprouting of GABAergic interneurons in temporal lobe epilepsy. *Epilepsy Behav.*, **7**, 390–400.

Behr, J., Gebhardt, C., Heinemann, U. & Mody, I. (2002) Kindling enhances kainate receptor-mediated depression of GABAergic inhibition in rat granule cells. *Eur. J. Neurosci.*, **16**, 861–867.

Bischofberger, J., Engel, D., Li, L., Geiger, J.R. & Jonas, P. (2006) Patch-clamp recording from mossy fiber terminals in hippocampal slices. *Nat. Protoc.*, **1**, 2075–2081.

Boyden, E.S., Zhang, F., Bamberg, E., Nagel, G. & Deisseroth, K. (2005) Millisecond-timescale, genetically targeted optical control of neural activity. *Nat. Neurosci.*, **8**, 1263–1268.

Brager, D.H., Luther, P.W., Erdelyi, F., Szabo, G. & Alger, B.E. (2003) Regulation of exocytosis from single visualized GABAergic boutons in hippocampal slices. *J. Neurosci.*, **23**, 10475–10486.

Cobb, S.R., Buhl, E.H., Halasy, K., Paulsen, O. & Somogyi, P. (1995) Synchronization of neuronal activity in hippocampus by individual GABAergic interneurons. *Nature*, **378**, 75–78.

Colmers, W.F., Lukowiak, K. & Pittman, Q.J. (1987) Presynaptic action of neuropeptide Y in area CA1 of the rat hippocampal slice. *J. Physiol.*, **383**, 285–299.

Deng, P.Y. & Lei, S. (2006) Bidirectional modulation of GABAergic transmission by cholecystokinin in hippocampal dentate gyrus granule cells of juvenile rats. *J. Physiol.*, **572**, 425–442.

Elmer, E., Kokaia, M., Kokaia, Z., Ferencz, I. & Lindvall, O. (1996) Delayed kindling development after rapidly recurring seizures: relation to mossy fiber sprouting and neurotrophin, GAP-43 and dynorphin gene expression. *Brain Res.*, **712**, 19–34.

Eslamboli, A., Georgievska, B., Ridley, R.M., Baker, H.F., Muzyczka, N., Burger, C., Mandel, R.J., Annett, L. & Kirik, D. (2005) Continuous low-level glial cell line-derived neurotrophic factor delivery using recombinant adeno-associated viral vectors provides neuroprotection and induces behavioral recovery in a primate model of Parkinson's disease. *J. Neurosci.*, **25**, 769–777.

Ferezou, I., Cauli, B., Hill, E.L., Rossier, J., Hamel, E. & Lambolez, B. (2002) 5-HT3 receptors mediate serotonergic fast synaptic excitation of neocortical vasoactive intestinal peptide/cholecystokinin interneurons. *J. Neurosci.*, **22**, 7389–7397.

Foldy, C., Lee, S.Y., Szabadics, J., Neu, A. & Soltesz, I. (2007) Cell type-specific gating of perisomatic inhibition by cholecystokinin. *Nat. Neurosci.*, **10**, 1128–1130.

Freedman, R., Wetmore, C., Stromberg, I., Leonard, S. & Olson, L. (1993) Alpha-bungarotoxin binding to hippocampal interneurons: immunocytochemical characterization and effects on growth factor expression. *J. Neurosci.*, **13**, 1965–1975.

Freund, T.F. (2003) Interneuron Diversity series: rhythm and mood in perisomatic inhibition. *Trends Neurosci.*, **26**, 489–495.

Freund, T.F. & Buzsaki, G. (1996) Interneurons of the hippocampus. *Hippocampus*, **6**, 347–470.

Freund, T.F. & Katona, I. (2007) Perisomatic inhibition. *Neuron*, **56**, 33–42.

Ghijsen, W.E., Leenders, A.G. & Wiegant, V.M. (2001) Regulation of cholecystokinin release from central nerve terminals. *Peptides*, **22**, 1213–1221.

Gruber, B., Greber, S., Rupp, E. & Sperk, G. (1994) Differential NPY mRNA expression in granule cells and interneurons of the rat dentate gyrus after kainic acid injection. *Hippocampus*, **4**, 474–482.

Gulyas, A.I., Hajos, N. & Freund, T.F. (1996) Interneurons containing calretinin are specialized to control other interneurons in the rat hippocampus. *J. Neurosci.*, **16**, 3397–3411.

Hefft, S. & Jonas, P. (2005) Asynchronous GABA release generates long-lasting inhibition at a hippocampal interneuron-principal neuron synapse. *Nat. Neurosci.*, **8**, 1319–1328.

Karson, M.A., Tang, A.H., Milner, T.A. & Alger, B.E. (2009) Synaptic cross talk between perisomatic-targeting interneuron classes expressing cholecystokinin and parvalbumin in hippocampus. *J. Neurosci.*, **29**, 4140–4154.

Kaspar, B.K., Erickson, D., Schaffer, D., Hinh, L., Gage, F.H. & Peterson, D.A. (2002) Targeted retrograde gene delivery for neuronal protection. *Mol. Ther.*, **5**, 50–56.

Katona, I., Sperlagh, B., Sik, A., Kafalvi, A., Vizi, E.S., Mackie, K. & Freund, T.F. (1999) Presynaptically located CB1 cannabinoid receptors regulate GABA release from axon terminals of specific hippocampal interneurons. *J. Neurosci.*, **19**, 4544–4558.

Klapstein, G.J. & Colmers, W.F. (1993) On the sites of presynaptic inhibition by neuropeptide Y in rat hippocampus in vitro. *Hippocampus*, **3**, 103–111.

Kobayashi, M. & Buckmaster, P.S. (2003) Reduced inhibition of dentate granule cells in a model of temporal lobe epilepsy. *J. Neurosci.*, **23**, 2440–2452.

Kofler, N., Kirchmair, E., Schwarzer, C. & Sperk, G. (1997) Altered expression of NPY-Y1 receptors in kainic acid induced epilepsy in rats. *Neurosci. Lett.*, **230**, 129–132.

Kokaia, M., Asztely, F., Olofsdotter, K., Sindreu, C.B., Kullmann, D.M. & Lindvall, O. (1998) Endogenous neurotrophin-3 regulates short-term plasticity at lateral perforant path-granule cell synapses. *J. Neurosci.*, **18**, 8730–8739.

Ledri, M., Sorensen, A.T., Erdelyi, F., Szabo, G. & Kokaia, M. (2011) Tuning afferent synapses of hippocampal interneurons by neuropeptide Y. *Hippocampus*, **21**, 198–211.

Marchal, C. & Mulle, C. (2004) Postnatal maturation of mossy fibre excitatory transmission in mouse CA3 pyramidal cells: a potential role for kainate receptors. *J. Physiol.*, **561**, 27–37.

Marksteiner, J., Ortler, M., Bellmann, R. & Sperk, G. (1990) Neuropeptide Y biosynthesis is markedly induced in mossy fibers during temporal lobe epilepsy of the rat. *Neurosci. Lett.*, **112**, 143–148.

McQuiston, A.R. & Colmers, W.F. (1996) Neuropeptide Y2 receptors inhibit the frequency of spontaneous but not miniature EPSCs in CA3 pyramidal cells of rat hippocampus. *J. Neurophysiol.*, **76**, 3159–3168.

Miles, R., Toth, K., Gulyas, A.I., Hajos, N. & Freund, T.F. (1996) Differences between somatic and dendritic inhibition in the hippocampus. *Neuron*, **16**, 815–823.

Monory, K., Massa, F., Egertova, M., Eder, M., Blaudzun, H., Westenbroek, R., Kelsch, W., Jacob, W., Marsch, R., Ekker, M., Long, J., Rubenstein, J.L., Goebbels, S., Nave, K.A., During, M., Klugmann, M., Wolfel, B., Dodt, H.U., Zieglgansberger, W., Wotjak, C.T., Mackie, K., Elphick, M.R., Marsicano, G. & Lutz, B. (2006) The endocannabinoid system controls key epileptogenic circuits in the hippocampus. *Neuron*, **51**, 455–466.

Nunzi, M.G., Gorio, A., Milan, F., Freund, T.F., Somogyi, P. & Smith, A.D. (1985) Cholecystokinin-immunoreactive cells form symmetrical synaptic contacts with pyramidal and nonpyramidal neurons in the hippocampus. *J. Comp. Neurol.*, **237**, 485–505.

Paredes, M.F., Greenwood, J. & Baraban, S.C. (2003) Neuropeptide Y modulates a G protein-coupled inwardly rectifying potassium current in the mouse hippocampus. *Neurosci. Lett.*, **340**, 9–12.

Porter, J.T., Cauli, B., Tsuzuki, K., Lambolez, B., Rossier, J. & Audinat, E. (1999) Selective excitation of subtypes of neocortical interneurons by nicotinic receptors. *J. Neurosci.*, **19**, 5228–5235.

Racine, R.J. (1972) Modification of seizure activity by electrical stimulation. II. Motor seizure. *Electroencephalogr. Clin. Neurophysiol.*, **32**, 281–294.

Scharfman, H.E. (1995) Electrophysiological evidence that dentate hilar mossy cells are excitatory and innervate both granule cells and interneurons. *J. Neurophysiol.*, **74**, 179–194.

Scharfman, H.E. (2007) The CA3 ''backprojection'' to the dentate gyrus. *Prog. Brain Res.*, **163**, 627–637.

Schwarzer, C., Kofler, N. & Sperk, G. (1998) Up-regulation of neuropeptide Y-Y2 receptors in an animal model of temporal lobe epilepsy. *Mol. Pharmacol.*, **53**, 6–13.

Somogyi, P. & Klausberger, T. (2005) Defined types of cortical interneurone structure space and spike timing in the hippocampus. *J. Physiol.*, **562**, 9–26.

Sorensen, A.T., Nikitidou, L., Ledri, M., Lin, E.J., During, M.J., Kanter-Schlifke, I. & Kokaia, M. (2009) Hippocampal NPY gene transfer attenuates seizures without affecting epilepsy-induced impairment of LTP. *Exp. Neurol.*, **215**, 328–333.

Stanic, D., Brumovsky, P., Fetissov, S., Shuster, S., Herzog, H. & Hokfelt, T. (2006) Characterization of neuropeptide Y2 receptor protein expression in the mouse brain. I. Distribution in cell bodies and nerve terminals. *J. Comp. Neurol.*, **499**, 357–390.

Traub, R.D., Pais, I., Bibbig, A., Lebeau, F.E., Buhl, E.H., Garner, H., Monyer, H. & Whittington, M.A. (2005) Transient depression of excitatory synapses on interneurons contributes to epileptiform bursts during gamma oscillations in the mouse hippocampal slice. *J. Neurophysiol.*, **94**, 1225–1235.

Tu, B., Jiao, Y., Herzog, H. & Nadler, J.V. (2006) Neuropeptide Y regulates recurrent mossy fiber synaptic transmission less effectively in mice than in rats: Correlation with Y2 receptor plasticity. *Neuroscience*, **143**, 1085–1094.

Vezzani, A., Sperk, G. & Colmers, W.F. (1999) Neuropeptide Y: emerging evidence for a functional role in seizure modulation. *Trends Neurosci.*, **22**, 25–30.

Ylinen, A., Soltesz, I., Bragin, A., Penttonen, M., Sik, A. & Buzsaki, G. (1995) Intracellular correlates of hippocampal theta rhythm in identified pyramidal cells, granule cells, and basket cells. *Hippocampus*, **5**, 78–90.

Zucker, R.S. & Regehr, W.G. (2002) Short-term synaptic plasticity. *Annu. Rev. Physiol.*, **64**, 355–405.